WARSAW UNIVERSITY OF TECHNOLOGY Index 351733
FACULTY OF CIVIL ENGINEERING
COMMITTEE FOR CIVIL AND WATER ENGINEERING
POLISH ACADEMY OF SCIENCES ISSN 1230-2945

DOI: 10.24425/ace.2025.153317

ARCHIVES OF CIVIL ENGINEERING

Vol. LXXI ISSUE 1 2025

pp. 5–18

Research paper

Design method of modular bi-directional load-bearing and energy dissipating joints in the context of intelligent construction

Hao Huang[1]

Abstract: The requirements for structural performance and seismic performance in the field of civil engineering are increasing. Traditional building structures have certain limitations in extreme conditions such as earthquakes. Therefore, this study discusses the design of modular bi-directional load-bearing and energy dissipating joints in the context of intelligent construction to improve the seismic performance of buildings. The study designs vertical joints and bi-directional joints, and the test results show that the hysteresis curve of the joints is hump-shaped, exhibiting excellent plastic deformation and energy dissipation performance. The introduction of oblique stiffening ribs in the vertical joints significantly improves the load-bearing capacity, and there is no significant decrease in load-bearing capacity when loaded to approximately 32 mm. The maximum energy dissipation coefficient of vertical joint specimen 1 is 1.485. For specimen 2, the maximum values is 1.801, and for the bi-directional joints, the maximum values is 2.156, demonstrating excellent energy dissipation capability. In conclusion, this research is of great significance for the combination of modern building engineering technology and intelligent construction, providing strong support for the seismic performance and overall safety of building structures.

Keywords: intelligent construction, modular, load-bearing and energy dissipation, seismic design, building structures

[1]A.P., SE., M.D., CHN., School of Civil Engineering, Guangxi Polytechnic of Construction, Nanning, 530007, China, e-mail: huanghao_gxnn@163.com, ORCID: 0009-0002-8495-7071

1. Introduction

Intelligent building is the use of modern science and information technology, to achieve a high degree of automation and digital building methods. It is gradually changing the way traditional construction projects are carried out and bringing revolutionary changes to the construction industry [1]. Modular construction is to manufacture prefabricated modules in the factory and then assemble them on site, which improves the construction speed and better ensures the control of construction quality [2]. However, earthquakes can cause serious damage to buildings, pose a threat to human life and property, and have a significant impact on social and economic stability [3]. Therefore, in this context, a new civil engineering design method – modular bidirectional load-bearing energy dissipation node is proposed. In this study, intelligent construction technology and seismic resistance are combined to design two new modular joints: vertical joints and bidirectional joints. Vertical connectors are used to achieve vertical connections between module components. The bidirectional joint realizes the vertical connection between the modules and ensures the horizontal stability between the modules. The aim of this study is to improve the performance of building structures under earthquake action, and to provide theoretical and practical basis for the integration of seismic design and intelligent construction technology in civil engineering.

2. Related work

Earthquake is a common destructive natural disaster, and seismic design has become a key research field in the field of civil engineering. Merino et al. proposed a solution based on dynamic time-history analysis and relative displacement floor response spectrum optimization to improve the seismic performance of buildings [4]. Kaveh et al. developed a performance-based seismic design optimization scheme, which provides a new approach for seismic building design [5]. O'Reilly et al. proposed a design framework based on expected annual losses, which provides an effective tool for early design decisions and better design schemes, thereby improving the overall seismic performance of buildings and reducing potential losses [6]. Filiatrault et al. proposed a displacement-based seismic design method to solve the coordination problem between structural and non-structural components in seismic design [7].

In the construction industry, modular design is one of the ways people are constantly looking for more efficient and sustainable building methods. Phocas et al. proposed a temporary spatial structure composed of parallel interconnected planar module rods to solve the problem of flexibility and adaptability of spatial structure [8]. Pan and Hon proposed a method called modular integrated construction to solve the challenges faced by high-density high-rise building construction, aiming to improve quality, productivity, safety and sustainability, and solve the problems encountered in high-rise building construction [9]. Stieler et al propose to integrate modularization and manufacturing steps into the design-to-production process to promote innovation in digital concrete manufacturing [10]. Marsault introduced the sunshine factor calculation meta-model for modular buildings, which provides an effective tool for architects to quickly evaluate building performance in the early stage of design [11].

3. Seismic modular load-bearing and energy dissipating joint construction and performance analysis

The modular load-dissipation joint plays a key role in seismic design. Two kinds of modular load-dissipation joint, vertical joint and bidirectional joint, are studied and designed.

3.1. Construction of vertical joints and Bi-directional joints

Modular load-bearing and energy dissipating joints are special structural elements used in seismic design. They can bear the load of the building and absorb and dissipate energy during earthquakes, thereby improving the seismic performance of the structure [12]. In this study, three-dimensional models of two types of modular load-bearing energy dissipation nodes were first constructed. The three-dimensional construction drawings of vertical nodes are shown in Figure 1.

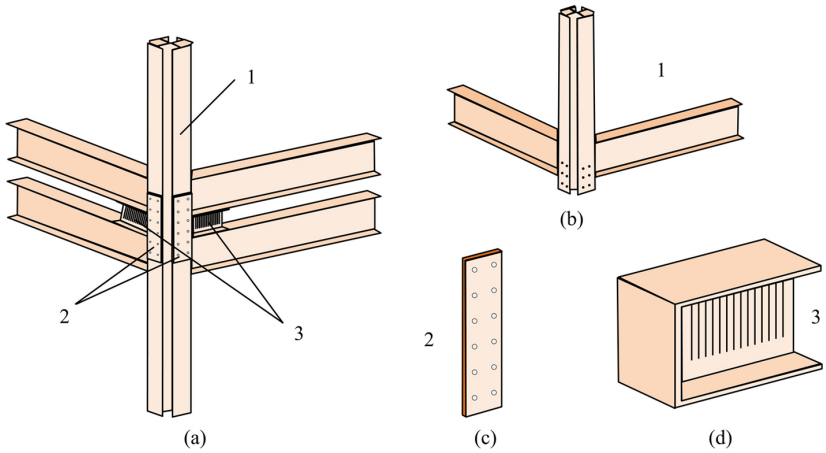

Fig. 1. 3D construction diagram of vertical joint: (a) Vertical node, (b) Top – Assemble module, (c) Connecting plate, (d) Vertical connector

Figure 1(a) is a vertical connection formed by connecting the upper and lower assembly modules with fully bolted vertical connectors. Figure 1(b) shows the upper assembly module unit, which is connected vertically through the lower flange of the floor beam to the bolt holes on the four sides of the column. Figure 1(c) shows the connection plate connected vertically. Figure 1(d) illustrates the vertical load-bearing connector, which consists of four steel plates. Connect the upper and lower assembly modules to form joints using fully bolted vertical connectors. The connecting plates are fixed directly with vertical bearing joints and bolted. The horizontal plate of the vertical bearing joint connects the upper flange of the ceiling to the lower flange of the floor beam. Vertical bearing connector plates increase connection stiffness. The vertical joint has high bearing capacity and seismic performance, and the whole bolted connection ensures the stability and safety of the building structure. The three-dimensional construction drawing of the bidirectional joint is shown in Figure 2.

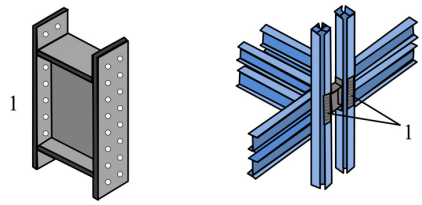

Fig. 2. 3D construction diagram of bidirectional joint: (a) Bidirectional node, (b) Nonnect 4 assembly modules

In Figure 2, the bidirectional node has both vertical and horizontal bidirectional connection functions. It consists of two vertical parts of the two-way connector, two horizontal parts of the two-way connector and a middle plate of the two-way connector, which can be assembled into a whole by welding or integral casting. The vertical part is bolted to the column flange and can be designed to protrude or flush. Intermediate plates can have openings or use small dampers. The combination of the bidirectional connector and the vertical connecting plate can realize the bidirectional connection of the assembled module. In addition, they can also be used to connect end-plate beams to achieve different architectural functions.

3.2. Mechanical model of vertical joints

Research on the mechanical properties of modular nodes is helpful to optimize the structural design and improve the overall stability [13]. There are three key assumptions in the establishment of the mechanical model of vertical joints. Firstly, it is assumed that the high-strength bolts connecting the modular units will not loosen during the elastic stage. Secondly, the connections at the joints are considered to be completely rigid during the elastic stage, without bending or sliding. Finally, the material and geometric properties of the beams and columns are taken from the points of contraflexure, which are the least prone to bending or stress concentration. The mechanical model of the vertical joint and the bending moment diagram are shown in Figure 3.

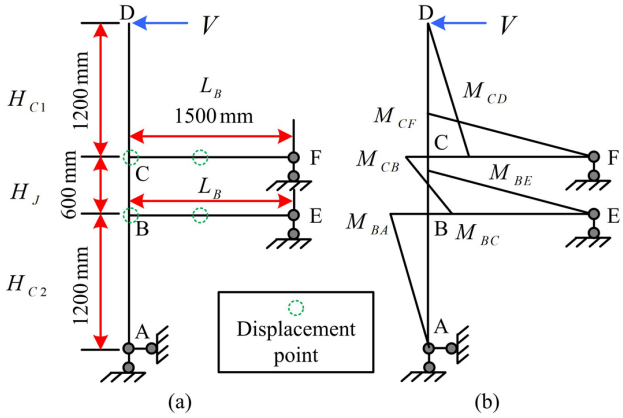

Fig. 3. Vertical joint mechanical feature and bending moment: (a) Mechanical model, (b) Bending moment

In Figure 3, V represents the horizontal push-over load at the column end, M represents bending moment, and the specific expression of bending moment of each section is shown in equation (3.1).

$$\begin{cases} M_{CD} = V \cdot H_{C1}, \quad M_{BA} = V \cdot H_{C2} \\ M_{DF} = V \cdot (H_{C1} + H_{C2} + H_{J1} + H_{J2} - \mu_V L_B) \\ M_{BE} = V \cdot \mu_V L_B, M_{BC} = V \cdot (H_{C2} - \mu_V L_B) \\ M_{CB} = V \cdot (H_{C2} + H_{J1} + H_{J2} - \mu_V L_B) \end{cases} \tag{3.1}$$

In equation (3.1), H_{C1} and H_{C2} represent the distance from the section centroid section at the column's end to the ceiling beam sections and floor beam sections centroids, respectively. H_{J1} represents the distance from the centroid of the floor beam section to the upper assembly module, and H_{J2} represents the distance from the centroid of the ceiling beam section to the lower assembly module. L_B represents the distance from the centroid of the section at the contraflexure points to the centroid of the column section. L_B is the vertical coefficient, which represents the proportional relationship between the sectional flexural stiffness and the length of the component in the vertical joint, as shown in equation (3.2).

$$\mu_V = \frac{\left[2\left(H_{C1} + H_{C2} + H_{J1} + H_{J2}\right) I_{jv} + \left(2H_{C2} + H_{J1} + H_{J2}\right) I_b^f\right] I_b^c}{L_B I_{jv} \left(I_b^f + I_b^c\right) + 3\left(H_{J1} + H_{J2}\right) I_b^f I_b^c} \tag{3.2}$$

In equation (3.2), I_{jv}, I_b^f, and I_b^c represent the inertia sectional moments for column connection segment, floor beam, and ceiling beam [14]. The vertical load-bearing and energy dissipating joint domain is more extensive compared to traditional joints, including the core areas P_M^f and P_M^c of the two assembly modules, the core areas P_C^f and P_C^c of the connection segments of the two assembly modules, and the mid-plate PU of the connector. Based on the bending moment diagram in Figure 4(b), the study uses the graph method to calculate the lateral displacement of the joint under the action of V. First, the lateral displacement Δ_{MV}^B caused by the bending of the assembly module beam is calculated, as shown in equation (3.3).

$$\Delta_{MV}^B = \frac{VH^2 L_B}{3EI_C} \left[\frac{\left(1 - \frac{\mu_V}{2}\right)^2 \cdot I_b^c + \left(\frac{\mu_V}{2}\right)^2 \cdot I_b^f}{I_b^c \cdot I_b^f} \right] \tag{3.3}$$

In equation (3.3), H represents the total height of the joint, and $H = H_{C1} + H_{C2} + H_{J1} + H_{J2}$. E represents the elastic modulus of the steel material, and I_C represents the moment of inertia of the assembly module section. Next, the lateral displacement Δ_{MV}^C caused by the bending of the assembly module column is calculated, as shown in equation (3.4).

$$\Delta_{MV}^C = V\left(H_{C1}^3 + H_{C2}^3\right)/3EI_C \tag{3.4}$$

Finally, the lateral displacement Δ_{MV}^F caused by the shear deformation of the core area P_M^f and P_M^c is calculated, as shown in equation (3.5).

$$\Delta_{MV}^F = V\left(H - h_J^f - h_J^c\right)/GA_C \tag{3.5}$$

In equation (3.5), h_J^f and h_J^c represent the heights of the core areas P_M^f and P_M^c, respectively. G represents the shear modulus of the steel material, and A_C represents the cross-sectional area of the column mid-plate. The total displacement $\Delta_{MV} = \Delta_{MV}^B + \Delta_{MV}^C + \Delta_{MV}^F$ of the vertical joint is then calculated, and its initial lateral stiffness K is given by equation (3.6).

$$K_{MV} = \frac{3EI_C I_b^c I_b^f A_C}{H^2 L_B I_C A_C \left[\left(1-\frac{\mu_V}{2}\right)^2 \cdot I_b^c + \left(\frac{\mu_V}{2}\right)^2 \cdot I_b^f\right] + \left(H_{C1}^3 + H_{C2}^3\right) I_b^c I_b^f A_C + 7.79\left(H - h_J^f - h_J^c\right)} \tag{3.6}$$

In equation (3.6), $G = \dfrac{E}{2(1+\nu)}$. ν represents the Poisson's ratio, with a value of 0.3, so $G = 0.385E$. In modular vertical joints, the core areas P_M^f and P_M^c undergo shear deformation under the column end load. Unlike traditional joints, one side of the core area is fixed while the other side is free. When the shear angle of the core area reaches the yield shear angle γ_y, only the column flange segment can bend in both directions to resist the horizontal load at the column end, while other parts are connected to the vertical connecting plate through bolts and cannot bend completely. Assuming that the core area P_B yields before the horizontal part of the connector, and the characteristics of the column sections of the upper and lower assembly modules remain consistent, the yield bearing capacity of the joint domain V_{py}^{MV} in the elastic stage is given by equation (3.7).

$$V_{py}^{MV} = 0.557F_y\,(0.95d_c t_{cw}) \cdot 2 \tag{3.7}$$

In equation (3.7), $0.557F_y$ comes from shear yield stress $\tau_y = \dfrac{F_y}{\sqrt{3}} = 0.557F_y$, F_y represents the yield strength of the steel material, and d_c and t_{cw} represent the width and thickness of P_M^f and P_M^c respectively, their reference sizes are 400 mm and 11 mm respectively. At this point, the yield shear angle γ_y^{MV} of the joint domain, with P_M^f and P_M^c having the same shear deformation direction, is represented as $\gamma_y^{MV} = 2\gamma_y$. One side of the core areas P_M^f and P_M^c is modeled as a spring with two corner points to resist the lateral load. For force equilibrium, it should satisfy $0.9d_b\gamma V = 2M\theta$. d_b, M, and θ represent the width, moment, and rotation angle of the column flange, respectively, where $\theta = \gamma$. Therefore, the lateral stiffness of the column flange can be obtained, as shown in equation (3.8).

$$K_{PF}^{MV} = \frac{V}{\gamma} = \frac{1.095b_c t_{cf}^2 G}{2d_{fb}}, \quad K_{PC}^{MV} = \frac{V}{\gamma} = \frac{1.095b_c t_{cf}^2 G}{2d_{cb}} \tag{3.8}$$

In equation (3.8), K_{PF}^{MV} and K_{PC}^{MV} represent the lateral stiffness of the column flange of P_M^f and P_M^c, respectively, d_{fb} and d_{cb} represent the height of P_M^f and P_M^c, their reference dimensions are all 180 mm, and b_c and t_{cf} represent the width and thickness of the column flange of the assembly module, their reference dimensions are 44 mm and 9 mm.

3.3. Bidirectional joint mechanical model

The assumptions for the bidirectional joint mechanical model include the neglect of high-strength bolt relaxation, rigid connection between the upper and lower columns, taking

the beams and columns from the points of contraflexure, and simplifying the analysis of the modular bidirectional load-bearing and energy dissipating joint for symmetric structures under asymmetric loads by using half of the structural model. The bidirectional joint mechanical model and the bending moment diagram are shown in Figure 4.

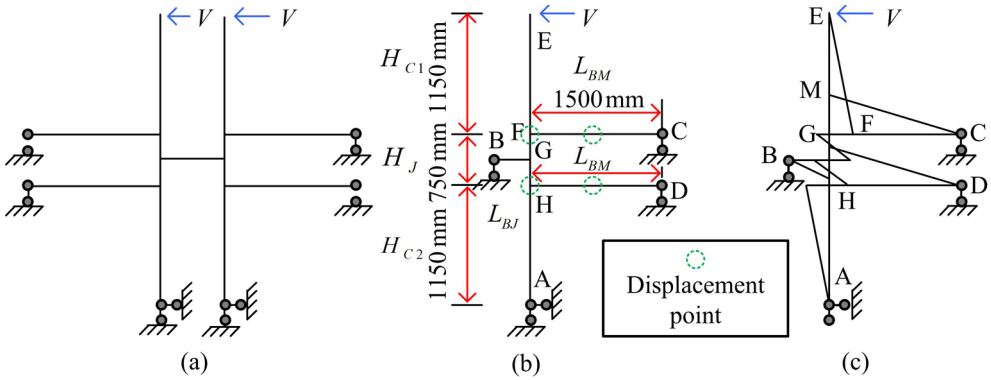

Fig. 4. Mechanical model of bidirectional joint and bending moment diagram: (a) Mechanical model, (b) Symmetrical structural mechanics model, (c) Bending moment diagram

In Figure 4, the bending moment expressions for each section are shown in equation (3.9).

$$
\begin{cases}
M_{FE} = VH_{C1}, \quad M_{FC} = V\mu_B L_{BM}, \quad M_{FC} = V\mu_B L_{BM} \\
M_{HD} = VL_{BM}\left(\dfrac{H}{L_{BJ}+L_{BM}} - \mu_B\right), \quad M_{GB} = V\dfrac{L_{BJ}H}{L_{BJ}+L_{BM}} \\
M_{FG} = V\left(\mu_B L_{BM} - H_{C1}\right), \quad M_{GF} = V\left[(H_{C1}+H_{J1}) - \mu_B L_{BM}\right] \\
M_{HG} = V\left(\mu_B L_{BM} + H_{C2} - \dfrac{HL_{BM}}{L_{BJ}+L_{BM}}\right) \\
M_{GH} = V\left(\dfrac{HL_{BM}}{L_{BJ}+L_{BM}} - H_{C2} - H_{J2} - \mu_B L_{BM}\right)
\end{cases} \tag{3.9}
$$

In equation (3.9), H_{C1}, H_{C2}, H_{J1}, H_{J2}, and H have the same meanings as in the vertical joint. L_{BM} and L_{BJ} represent the gap starting with the ceiling beam and floor beam contraflexure points to the column section centroid, and the distance from the centroid of the bidirectional connector section to the centroid of the column section, respectively. μ_B represents the bidirectional coefficient, as expressed in equation (3.10).

$$
\mu_B = \frac{\left\{2I_{jb}L_{BM}^2 H + 3I_b^c L_{BJ}\left[H_{J1}(2H_{C1}+H_{J1}) - H_{J2}(2H_{C2}+H_{J2})\right]\right\} I_b^f}{2L_{BJ}L_{BM}\left[I_{jb}\left(I_b^f + I_b^c\right)L_{BM} + 3I_b^f I_b^c (H_{J1}+H_{J2})\right]} \tag{3.10}
$$

In equation (3.10), I_{jb}, I_b^f, and I_b^c represent the inertia sectional moments for column connection segment, floor beam, and ceiling beam, respectively. The bidirectional joint has a total of 9 core areas, including the core areas P_M^{rf}, P_M^{rc}, P_C^{rf}, and P_C^{rc} of the upper right,

lower right, upper left, and lower left assembly module joints, the core areas P_C^{rc}, P_M^{lc}, P_C^{lf}, and P_C^{lc} of the upper left and lower left assembly module joints, and the mid-plate P_{BM}. First, the lateral displacement Δ_{MB}^{B} caused by the bending of the assembly module beam is calculated, as shown in equation (3.11).

$$\Delta_{MB}^{B} = \frac{VL_{BM}^{3}}{3E}\left[\frac{\left(\frac{H}{L_{BJ}+L_{BM}}-\mu_B\right)^2\cdot I_b^c+(\mu_B)^2\cdot I_b^f}{I_b^f I_b^c}\right] \tag{3.11}$$

In equation (3.11), H represents the total height of the joint. $H = H_{C1} + H_{C2} + H_{J1} + H_{J2}$. E represents the elastic modulus of the steel material. The lateral displacement Δ_{MB}^{C} caused by the bending of the assembly module column is calculated as shown in equation (3.12).

$$\Delta_{MB}^{C} = \frac{V\left(H_{C1}^3+H_{C2}^3\right)}{3EI_{mc}} \tag{3.12}$$

In equation (3.12), I_{mc} represents the moment of inertia of the assembly module column section. Finally, the lateral displacement Δ_{MB}^{J} caused by the shear deformation of the core areas P_M^{rf} and P_M^{rc} is calculated as shown in equation (3.13).

$$\Delta_{MB}^{J} = \frac{V\left(H\cdot\frac{L_{BM}}{L_{BJ}+L_{BM}}-h_J^f-h_J^c\right)}{GA_{mc}} \tag{3.13}$$

In equation (3.13), h_J^f and h_J^c represent the heights of the core areas P_M^{rf} and P_M^{rc}, respectively. G represents the shear modulus of the steel material, and A_{mc} represents the cross-sectional area of the column mid-plate. The total displacement of the vertical joint is $\Delta_{MV} = \Delta_{MB}^{B} + \Delta_{MB}^{C} + \Delta_{MB}^{J}$. Its initial lateral stiffness K_{MV} is given by equation (3.14).

$$K_{MV} = \frac{V}{\Delta_{MB}} = \frac{3EI_b^cI_b^fI_{mc}A_{mc}}{H^2L_{MB}I_{mc}A_{mc}\left[\left(1-\frac{\mu_B}{2}\right)^2\cdot I_b^c+\left(\frac{\mu_B}{2}\right)^2\cdot I_b^f\right]+\left(H_{C1}^3+H_{C2}^3\right)I_b^cI_b^fA_{mc}+7.79\left(H-h_J^f-h_J^c\right)} \tag{3.14}$$

In equation (3.14), $G = \frac{E}{2(1+\nu)}$. ν represents the Poisson's ratio, with a value of 0.3, so $G = 0.385E$. In the elastic stage, the yield bearing capacity V_{py}^{MB} of the joint domain is given by equation (3.15).

$$V_{py}^{MB} = 0.557F_y\left(0.95d_ct_{cw}\right)\cdot 2 \tag{3.15}$$

In equation (3.15), F_y represents the yield strength of the steel material, and d_c and t_{cw} represent the width and thickness of P_M^{rf} and P_M^{rc}, their reference sizes are 340 mm and 9 mm respectively.

4. Experimental study of the joints

To test the seismic performance of the designed joints, the study conducted experimental research on the vertical joints and bidirectional joints from four perspectives.

4.1. Experimental study on spatial loading of vertical joints

Two full-size modular vertical load-bearing energy dissipation nodes, specimen 1 and specimen 2, were designed for the experimental study of space cyclic load under bidirectional earthquake action. The lower assembly module ceiling beam flange of specimen 2 is welded with diagonal stiffened plates. The beam end loading method is studied, and the three-jack loading system is adopted. In this study, the hysteresis curves of two specimens were tested first. The hysteretic curves of the 1#Double beam and 2#Double beam of specimen 1 under cyclic loading are shown in Figure 5.

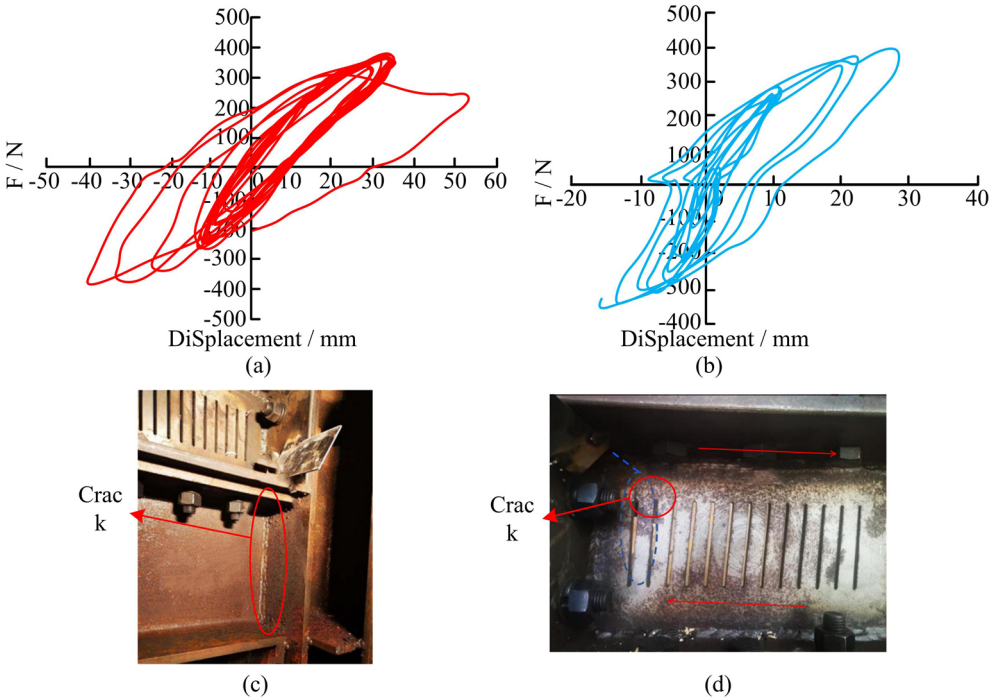

Fig. 5. Hysteresis curve of specimen 1: (a) 1#Double beam, (b) 2#Double beam, (c) 1#Double beam crack, (d) 2#Double beam crack

In Figure 5, the hysteresis curve of the vertical load-bearing energy-consuming node presents a full loop, indicating that it has strong plastic deformation and strong seismic energy-consuming capacity. Under vertical upward load, the weld seam between the lower flange of the 2# double beam suspended ceiling beam and the flange of the column cracks,

and the displacement is 29.24 mm, but the bearing capacity does not decrease significantly. The weld between the lower flange of the ceiling beam and the column flange of the 1#Double beam cracks due to vertical upward load, resulting in a sharp decrease in bearing capacity and stop loading. The hysteresis curve of specimen 2 is shown in Figure 6.

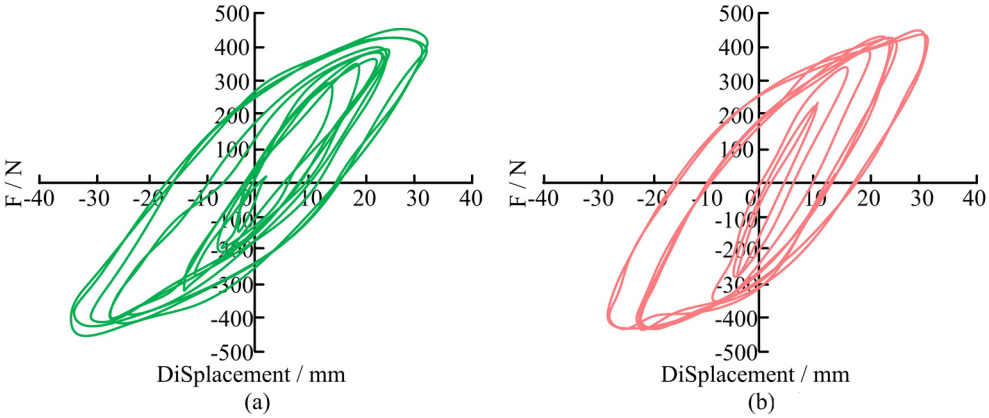

Fig. 6. Hysteresis curve of specimen 2: (a) 1#Double beam, (b) 2#Double beam

In Figure 6, the hysteresis curves of the 1#Double beam and 2#Double beam of specimen 2 present a complete hysteresis loop shape and have good plastic deformation and energy dissipation capacity. At the initial stage of loading, the node hysteresis curve presents a slight asymmetry, but with the continuation of loading, the hysteresis curve gradually becomes stable and regular. The inclined reinforcement design of specimen 2 significantly improves its bearing capacity. When the displacement is about 32 mm, its bearing capacity does not decrease significantly. The stiffness degradation curves of Specimen 1 and Specimen 2 are shown in Figure 7.

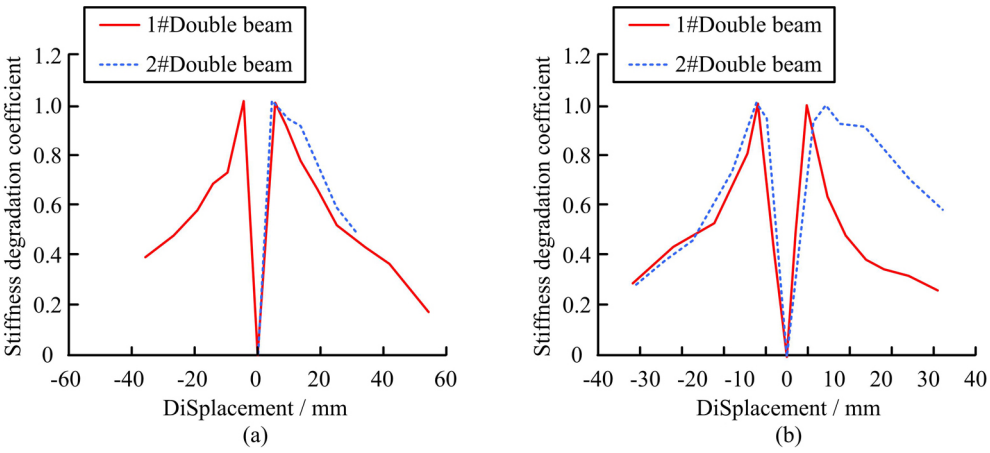

Fig. 7. Stiffness degradation curves of specimens 1 (a) and 2 (b)

From Figure 7, the stiffness degradation trend of each double beam in the test is relatively flat. At the beginning of the test, the stiffness degradation of specimens 1 and 2 was not significant, but once they entered the plastic deformation state, the stiffness degradation coefficients of the double beams 1# and 2# began to decline at different speeds. However, the 2#Double beam tie rod displacement meter in specimen 1 was disturbed by oblique load and could not be analyzed in detail. In specimen 2, the stiffness degradation coefficients of double beams 1# and 2# decreased slightly after they entered the plastic deformation state, but they were also disturbed by the oblique load. Finally, the energy dissipation performance of vertical nodes is tested, and the results are shown in Table 1.

Table 1. Energy dissipation performance test results of vertical joints

Test specimen	Double beam	E_i
Specimen 1	1#Double beam	1.485
	2#Double beam	1.326
Specimen 2	1#Double beam	1.801
	2#Double beam	1.691

In Table 1, E_i represents the energy dissipation coefficient. Under the reciprocating load, the maximum E_i of specimen 1 is 1.485, and the maximum E_i of specimen 2 is 1.801, indicating that the vertical joints have good energy dissipation performance. However, due to the cracking of the stiffeners and weld between the flange of the column, the 2#Double beam of Specimen 1 stopped loading at 29.74 mm, resulting in lower energy dissipation coefficient.. On the contrary, the addition of strengthening plates on the 1# and 2#Double beams of Specimen 2 improved the energy dissipation performance, making it superior to Specimen 1.

4.2. Experimental study on planar loading of bidirectional joints

For the experimental study on planar cyclic loading of bidirectional joints, four assembly module units were used, each consisting of a column and a beam welded vertically to the column. The beams were loaded at their ends, taking into account the constraints of the double columns and the continuous application of axial compression, while also applying reverse loading to simulate the seismic performance of the joints. The hysteresis curves were first tested, and the results are shown in Figure 8.

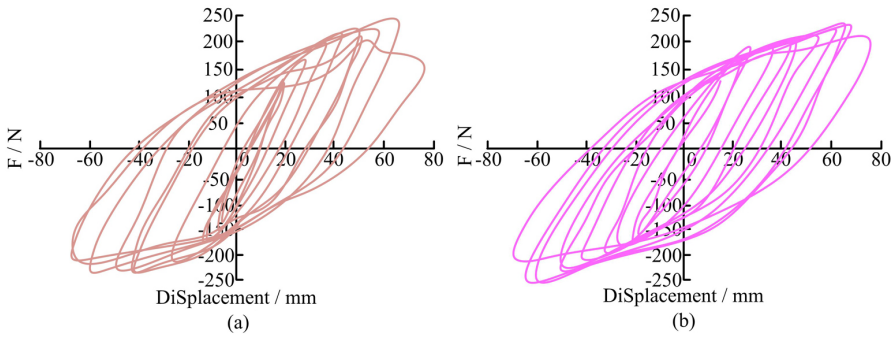

Fig. 8. Hysteresis curves of specimen: (a) 1#Double beam, (b) 2#Double beam

From Figure 8, it can be seen that the hysteresis curves of the 1#Double beam and 2#Double beam exhibit a hysteresis loop shape, indicating excellent energy dissipation capacity of the specimens. In the experiment, when the 1# ceiling beam was subjected to vertical upward loading, the weld between the lower flange of the beam and the flange of the column cracked, and at the same time, diagonal tearing of the web occurred in the direction of the applied force, resulting in a sharp decrease in load-bearing capacity on the hysteresis curve. The upper flange of the 1# floor beam also experienced local yielding. Meanwhile, under downward loading, the upper flanges of the 2# ceiling beam and 2# floor beam of Specimen 2 exhibited significant bending and a decrease in load-bearing capacity, and the upper flange of the 2# floor beam also showed noticeable buckling. Finally, the stiffness degradation curves and energy dissipation performance of the specimens were tested, and the results are shown in Figure 9.

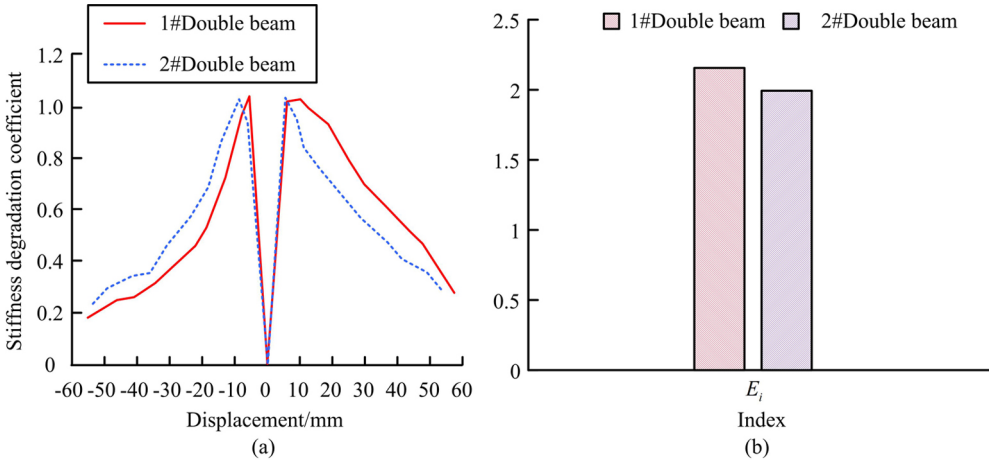

Fig. 9. Stiffness degradation curve and energy dissipation performance of specimen: (a) Stiffness degradation curve, (b) Energy dissipation performance test results

From Figure 9, the stiffness degradation patterns of the specimens in both positive and negative directions are similar, experiencing horizontal linear segments, linear descending segments, and curved descending segments. The horizontal linear segment represents the elastic stage, where the stiffness remains relatively constant. The degradation of stiffness mainly occurs after the yield point of the specimens due to the accumulation of plastic deformation. When compressive force is applied, the stiffness of the specimens sharply decreases after yielding, but as the horizontal displacement load increases, the degradation rate gradually decreases. The E_i under cyclic loading for the 1# and 2#Double beams is 2.156, indicating that the modular bidirectional load-bearing and energy dissipation joints have strong energy dissipation capacity when the four module units are connected bidirectionally and the critical parts of the columns are discontinuous.

5. Conclusions

In view of the lack of seismic performance of traditional buildings, this paper explores the seismic design method of modular two-way load-bearing energy dissipation joints. The vertical and bidirectional nodes are designed and their mechanical models are discussed. The load bearing performance and energy dissipation performance were evaluated by experiments. The test results show that the hysteretic curve of the vertical bearing energy dissipation joint is looped, which indicates that it has strong plastic deformation and strong seismic energy dissipation ability. Among them, after the introduction of inclined stiffener design, the bearing capacity of specimen 2 is significantly improved, and it does not decrease significantly until the displacement is about 32 mm. Under the reciprocating load, the maximum E_i of specimen 1 is 1.485, and that of specimen 2 is 1.801, indicating that the vertical joints have good energy dissipation performance. The bidirectional node has good ductility. The cyclic load of 1# and 2#Double beams is 2.156, and the energy dissipation capacity is strong. In summary, this study provides an important reference and experimental basis for improving the seismic performance of building structures. However, there is a lack of experimental analysis on the relationship between the regional shear Angle and the shear capacity of vertical and bidirectional joints, which is worthy of further study in the follow-up experiments.

Acknowledgements

The research is supported by Guangxi Science and Technology Program (Guike AD23026265); 2022 Guangxi University Young and Middle-aged Teachers Research Basic Ability Improvement Project “Research on Application of Digital Twin Technology in Safety Management Diagnosis of Guangxi Construction Projects” (2022KY1165).

References

[1] C.J. Turner, J. Oyekan, L. Stergioulas, and D. Griffin, “Utilizing industry 4.0 on the construction site: Challenges and opportunities”, *IEEE Transactions on Industrial Informatics,* vol. 17, no. 2, pp. 746–756, 2021, doi: 10.1109/TII.2020.3002197.

[2] J. Guo, T. Suma, J.J. Richardson, and H. Ejama, “Modular assembly of biomaterials using polyphenols as building blocks”, *ACS Biomaterials Science and Engineering*, vol. 5, no. 11, pp. 5578–5596, 2019, doi: 10.1021/acsbiomaterials.8b01507.

[3] D.J. Wald, “Practical limitations of earthquake early warning”, *Earthquake Spectra*, vol. 36, no. 3, pp. 1412–1447, 2020, doi: 10.1177/8755293020911388.

[4] R.J. Merino, D. Perrone, and A. Filiatrault, “Consistent floor response spectra for performance-based seismic design of nonstructural elements”, *Earthquake Engineering and Structural Dynamics*, vol. 49, no. 3, pp. 261–284, 2020, doi: 10.1002/eqe.3236.

[5] A. Kaveh, L. Mottaghi, and R.A. Izadifard, “An integrated method for sustainable performance-based optimal seismic design of RC frames with non-prismatic beams”, *Scientia Iranica*, vol. 28, no. 5, pp. 2596–2612, 2021, doi: https://doi.org/10.1177/8755293020911388.

[6] G.J. O’Reilly and G.M. Calvi, “Conceptual seismic design in performance-based earthquake engineering”, *Earthquake Engineering and Structural Dynamics*, vol. 48, no. 4, pp. 389–411, 2019, doi: 10.1002/eqe.3141.

[7] A. Filiatrault, D. Perrone, R.J. Merino, and G.M. Calvi, “Performance-based seismic design of nonstructural building elements”, *Journal of Earthquake Engineering*, vol. 25, no. 2, pp. 237–269, 2021, doi: 10.1080/13632469.2018.1512910.

[8] M.C. Phocas, M. Matheou, A. Müller, and E.G. Christoforou, "Reconfigurable modular bar structure", *Journal of the International Association for Shell and Spatial Structures*, vol. 60, no. 1, pp. 78–89, 2019, doi: 10.20898/j.iass.2019.199.028.

[9] W. Pan and C.K. Hon, "Briefing: Modular integrated construction for high-rise buildings", *Proceedings of the Institution of Civil Engineers-Municipal Engineer*, vol. 173, no. 2, pp. 64–68, 2020, doi: 10.1680/jmuen.18.00028.

[10] D. Stieler, T. Schwinn, and A. Menges, "Volumetric intersections: Modularization approaches for freeform prefab concrete construction", *Civil Engineering Design*, vol. 4, no. 1-3, pp. 3–13, 2022, doi: 10.1002/cend.202100047.

[11] X. Marsault, "Achieving realtime daylight factor computation for modular buildings in generative design", *Journal of Building Performance Simulation*, vol. 15, no. 6, pp. 848–865, 2022, doi: 10.1080/19401493.2022.2102676.

[12] J. Zhang and R. Yan, "Centralized energy-efficient clustering routing protocol for mobile nodes in wireless sensor networks", *IEEE Communications Letters*, vol. 23, no. 7, pp. 1215–1218, 2019, doi: 10.1109/LCOMM.2019.2917193.

[13] A. Bubshait and B. Jha, "Coupled poromechanics-damage mechanics modeling of fracturing during injection in brittle rocks", *International Journal for Numerical Methods in Engineering*, vol. 121, no. 2, pp. 256–276, 2020, doi: 10.1002/nme.6208.

[14] M. Ren, T. Li, K. Shi, P. Xu, and Y. Sun, "Coordinated control strategy of virtual synchronous generator based on adaptive moment of inertia and virtual impedance", *IEEE Journal on Emerging and Selected Topics in Circuits and Systems*, vol. 11, no. 1, pp. 99–110, 2021, doi: 10.1109/JETCAS.2021.3051320.

Received: 2024-01-02, Revised: 2024-04-30